AAS 16-245

SURROGATE MODEL FOR PROBABILISTIC MODELING OF ATMOSPHERIC ENTRY FOR SMALL NEO'S

Piyush M. Mehta[*], Martin Kubicek[†], Edmondo Minisci[‡], and Massimiliano Vasile[§]

Near Earth Objects (NEOs) enter the Earths atmosphere on a regular basis. Depending on the size, object and entry parameters; these objects can burn-up through ablation (complete evaporation), undergo fragmentation of varying nature, or impact the ground unperturbed. Parameters that influence the physics during entry are either unknown or highly uncertain. In this work, we propose a probabilistic approach for simulating entry. Probabilistic modeling typically requires an expensive Monte Carlo approach. In this work, we develop and present a novel engineering approach of developing surrogate models for simulation of the atmospheric entry accounting for drag, ablation, evaporation, fragmentation, and ground impact.

INTRODUCTION

Near Earth Objects (NEOs) are defined as objects in the solar system that have a close proximity to Earth during some part of their orbital motion around the Sun. NEOs can be further classified as asteroids, comets or meteoroids. Asteroids are large rocky bodies that are formed in the inner solar system, while comets are formed in the outer planetary system. Meteoroids are smaller versions of asteroids. Asteroid sized objects entering the Earth's atmosphere for impact can have global implications with the possibility of causing extinction type events. Depending on the size, meteoroids entering the Earth's atmosphere can either evaporate (called meteor or shooting star) or survive, fragment and reach the ground (called meteorites).

Current work concentrates on small asteroids and large meteoroids (up to 20m in size). Figure 1 shows the distribution of the small objects that have entered the Earth's atmosphere over the last two decades. Depending mainly on the material composition of the entering objects, they can undergo disintegration under different scenarios such as an air-burst or mechanical fragmentation. In an air-burst, the object typically disintegrates into dust like clouds while releasing significant energy causing secondary effects such as a heat and/or a shock wave. In mechanical fragmentation, the object disintegrates into smaller pieces under aerodynamic stresses.

Small-to-medium sized NEOs are unlikely to cause global-scale events but can pose an infrequent, but very real threat to life and property on Earth. On February 15, 2013, an asteroid entered Earth's atmosphere with a velocity of approximately 65,000 km/h and exploded at around 25 km altitude due to the heating and stresses. The asteroid was estimated to have a diameter of 18m and

[*]Marie Curie Fellow, Mech. and Aerospace Engineering, University of Strathclyde, 75 Montrose Street, Glasgow G1 1XJ.
[†]PhD Candidate, Mech. and Aerospace Engineering, University of Strathclyde, 75 Montrose Street, Glasgow G1 1XJ.
[‡]Lecturer, Mech. and Aerospace Engineering, University of Strathclyde, 75 Montrose Street, Glasgow G1 1XJ.
[§]Professor, Mech. and Aerospace Engineering, University of Strathclyde, 75 Montrose Street, Glasgow G1 1XJ.

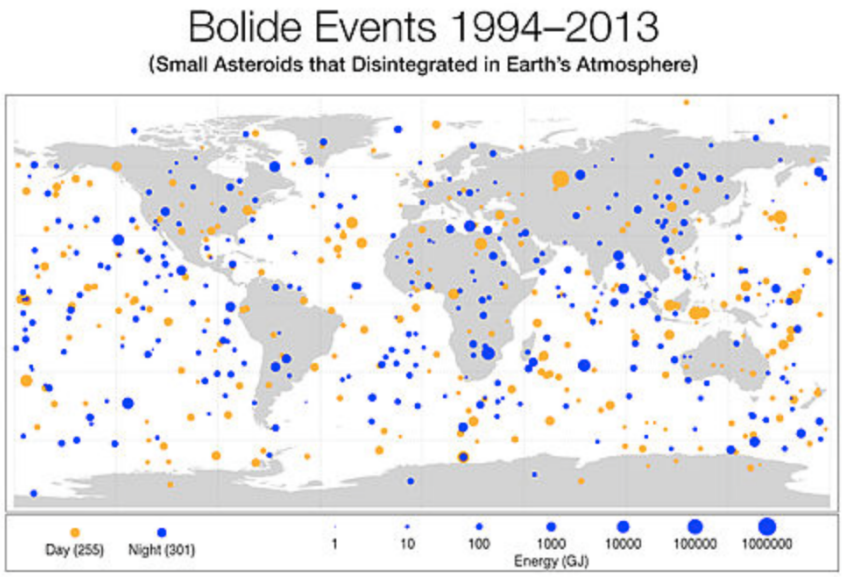

Figure 1: Statistics of Small Asteroid Impact over last 2 decades (courtesy JPL)

a mass of 11,000 tons. The total energy released to the atmosphere was around 500 kilotons of TNT. The explosion resulting from the immense heating during atmospheric entry resulted in a heat wave and a strong shock wave shattering glass across several miles with approximately 1500 people requiring medical attention. The air-burst also resulted in several small-to-large fragments reaching the ground, the largest one weighing in at nearly half a ton. Such an event is estimated to occur roughly on average once every 100 years.[1,2,3,].[4] On the same day, another asteroid 2012DA14 with a diameter of approximately 40 m passed by the Earth at an altitude of only 28,000 km. Impact of asteroids of this size are expected roughly on average every 1000 years.[1,2,3,4]

The meteoroid community also follows closely the medium sized objects that enter the Earth's atmosphere. The analysis of surviving fragments on ground can provide significant insights and knowledge about family and origin of such objects as well as improve our understanding of the NEO population. Scientists believe that the recovered fragments can provide insights into several open scientific questions such as the origin of life. Survivability and surface impact location of NEOs entering the Earth's atmosphere is dictated by, among other things, the atmospheric entry conditions, atmospheric properties and asteroid properties. High fidelity numerical simulations using 2D and 3D hydrodynamical codes have been performed that provide great insights into the physical evolution of the object as it travels through the atmosphere[5,6,7,8,9,].[10] However, these simulations are highly expensive in nature and can be performed only for a limited number of cases.

Unfortunately, almost all parameters that affect survivability and trajectory are uncertain and require uncertainty quantification and propagation (UQ&P) for realistic modeling of the effects on ground. A Monte Carlo approach was recently applied to the problem; however, the computational requirement of such a simulation is very high.[11] An approach based on high dimensional model representation (HDMR) and derivative based uncertainty quantification[12] was recently applied to the re-entry of debris objects, however, the work did not include any physics for ablation and fragmentation.[13]

In this work, a novel approach that uses the HDMR approach in combination with surrogate modeling for the physical events is developed and presented. More precisely, the HDMR technique is used to learn and generalize the dynamics and evolution of the entering objects through the atmosphere, to predict in a very fast way the final state of the objects at any major events, such as fragmentation, total evaporation, or impact on ground. Such an analysis accounting for the uncertainties that can affect the physical evolution of the atmospheric entry as well as knowledge about the possible distribution of the impact location can be used towards provide advance warnings to local governments for decision making. Current work is restricted to modeling mechanical fragmentation, however, the modular nature of the developed method/tool allows easy swapping of physical models to consider worst case scenario under all possible conditions. The goal is to have a tool that can be accessed and run using the resources of a web interface, allowing each access to the tool from anywhere around the world.

The paper is structured in the following manner. The section described in the detail the methodology including the dynamic and physical models as well the mathematical formulation of the HDMR approach and model development. The following section compares the results from the HDMR with a Monte Carlo simulation run. The final sections provides conclusions for the current work and insights into future work.

METHODOLOGY

We begin the atmospheric entry simulation at an altitude of 120 km. The shape of the object is expected to affect the dynamics, however, due to the highly uncertain nature of the NEO characteristics and the lack of knowledge of the physics for modeling of fragmentation, both the original parent and subsequent fragments are modeled as spherical objects. The original parent object is tracked through the atmosphere either down to ground or evaporation due to ablation. Ablation due to convective and radiative heat transfer is modeled. Radiative and convective heat fluxes are calculated through a combination of experimental/computational data and analytical models.[14] The ablation model as described by Bronshten[15] is used where the effective heat transfer is calculated and translated to rate of change of mass.

Fragmentation criteria as developed by Tsvetkov and Skripnik[16] is used to model fragmentation events. Successive fragmentation events are modeled where the smaller fragment is given a lateral velocity for separation while the perturbed trajectory of the larger fragment is computed under the conservation of momentum.[17] The lateral velocity depends on the relative orientation of the two fragments,[17] however, it is impossible to accurately predict the relative position. Ablation and fragmentation criteria are applied to each subsequent fragment. All subsequent fragment objects are also tracked either to ground impact or evaporation. Figure 2a and 2b show a schematic of the trajectory propagation with fragmentation and ablation and a schematic of the planar entry, respectively. Figure 2c shows the algorithm developed for the simulation.

Trajectory Dynamics Model

The object entering the Earth's atmosphere is modeled as a point mass whose dynamics is governed by the following system of differential equations:

$$\dot{h} = V \sin\gamma \tag{1}$$

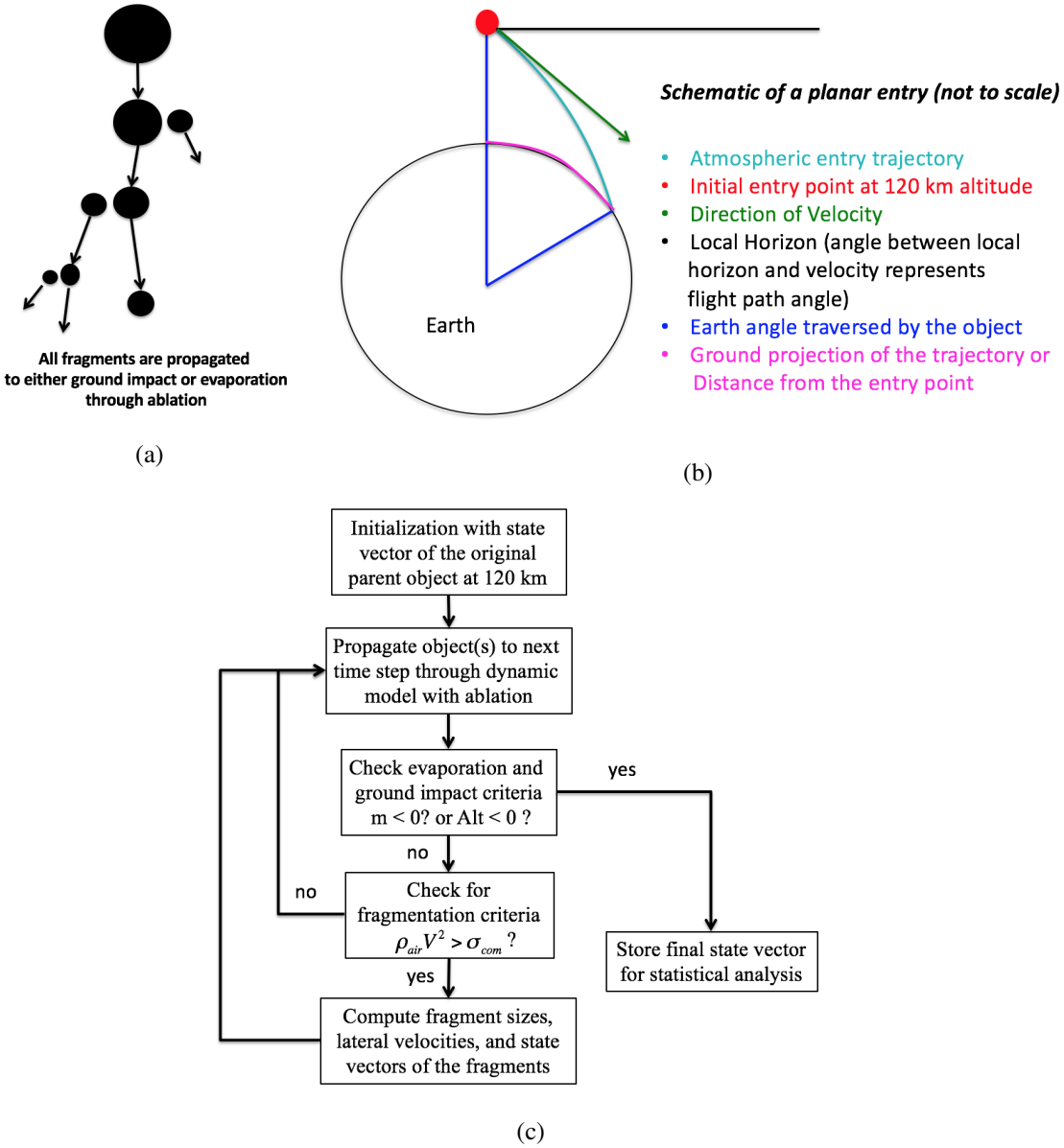

Figure 2: (a) A schematic of the trajectory simulation with fragmentation and ablation, (b) schematic of a planar entry, and (c) developed algorithm for the simulation.

$$\dot{V} = -\frac{D}{m} - g\sin\gamma + \omega_E^2\left(R_E + h\right)\cos\phi\left(\sin\gamma\cos\phi - \cos\gamma\cos\chi\sin\phi\right) \tag{2}$$

$$\dot{\gamma} = \left(\frac{V}{R_E + h} - \frac{g}{V}\right)\cos\gamma + 2\omega_E\sin\chi\cos\phi + \omega_E^2\left(\frac{R_E + h}{V}\right)\cos\phi\left(\cos\chi\sin\gamma\sin\phi + \cos\gamma\cos\phi\right) \tag{3}$$

$$\dot{\chi} = -\left(\frac{V}{R_E + h}\right)\cos\phi\sin\chi\tan\phi + 2\omega_E\left(\sin\phi - \cos\chi\cos\phi\tan\gamma\right) - \omega_E^2\left(\frac{R_E + h}{V\cos\gamma}\right)\cos\phi\sin\gamma\sin\chi \quad (4)$$

$$\dot{\phi} = \left(\frac{V}{R_E + h}\right)\cos\gamma\cos\chi \quad (5)$$

$$\dot{\lambda} = \left(\frac{V}{R_E + h}\right)\frac{\cos\gamma\sin\chi}{\cos\phi} \quad (6)$$

where h is the altitude, V is the speed of the object, γ is the flight path angle, D is the drag force, g is the gravitational acceleration, ω_E is the Earth's rotational speed, R_E is the radius of the Earth, χ is path direction angle, and ϕ and λ are latitude and longitude, respectively. The gravitation acceleration is modeled as a function of the altitude given as:

$$g\left(h\right) = g_0\left(\frac{h}{R_E + h}\right)^2 \quad (7)$$

where the values of g_0 is 9.81 ms^{-2}.

Hypersonic Aerodynamics

A simple sphere model is used for the object geometry. Since most of the atmospheric entry occurs at the high hypersonic regime where the drag coefficient is independent of the value of the Mach number, we assume a value of 0.92 for the drag coefficient given by Simplified Newtonian Theory in the continuum regime.[18] We use a drag coefficient value of 2.2 for the free molecular regime. In the transition regime, we use a recently developed bridging function model for drag coefficient as a function of local Knudsen number (Kn).[19] Again, the proposed probabilistic analysis is assumed to mitigate the uncertainties associated with the models used to compute the drag coefficient. Acceleration due to drag acting on the object used in Eq. 8 is calculated using the standard theoretical drag model given as:

$$a_{drag} = \frac{D}{m} = -\frac{1}{2}\rho_{air}\frac{C_D A}{m}V^2\frac{V}{|V|} \quad (8)$$

where ρ_{air} is the atmospheric density, C_D is the drag coefficient, A is the cross sectional area, and m is the mass of the object. Since the entering object is modeled as a sphere, we assume the nature of the motion to be planar (lift and side forces are neglected). It should be noted however, that the developed framework is modular in nature allows for easy addition of lift and side forces by implementing small changes in the dynamics model.

Atmospheric Density The atmospheric density, ρ_{air}, is computed using an interpolation routine that is developed using data from the US standard atmosphere.[20] Values (mean and boundaries for 99% of all samples) at a series of altitudes are obtained from the US standard atmosphere. We assign Gaussian distributions to the data at these altitudes, which allow draws from the distributions for every Monte Carlo sample. Densities at altitudes other than those with data points are computed

using piece-wise linear interpolation in the logarithmic scale. The values in the US standard atmosphere are provided to an altitude of about 90 km. The mean value at 120 km was read of the US standard atmosphere table and the boundaries were assumed to be the same as at 90 km. Figure 3 shows 1000 samples drawn from the density interpolation routines, constrained to the data points. Every run of the Monte Carlo sample uses one of the data lines shown in Figure 3 for propagation of trajectory from entry to ground.

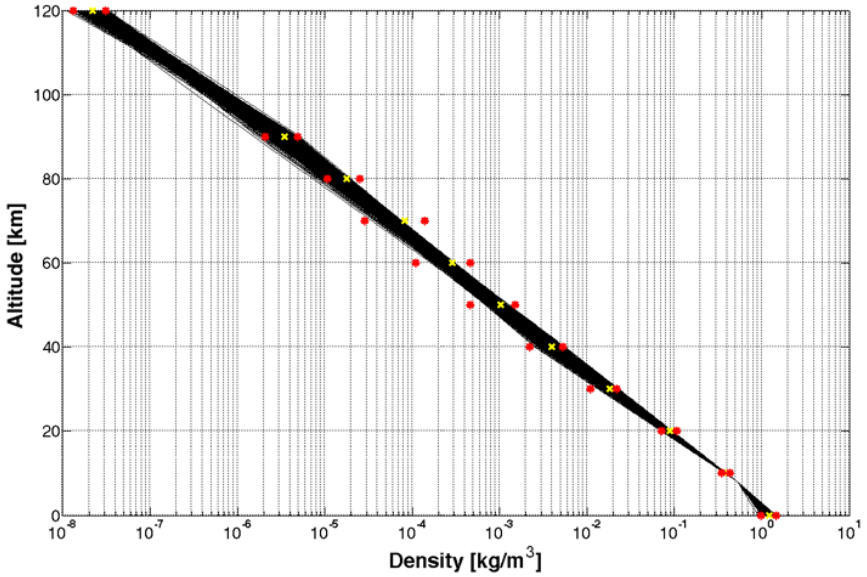

Figure 3: 1000 samples from the density interpolation routine. The yellow and red data points represent the mean and boundaries for 99% of all samples, respectively.

Ablation Model

The rate at which the object material mass is ablated is calculated using the following relationship:

$$\dot{m} = -\frac{(Q_R + Q_C)}{Q_{ab}} \tag{9}$$

where Q_{ab} is the effective heat of ablation, and Q_R and Q_C are effective radiative and convective heat transfer values, respectively. Brandis et al.,[14] give the correlations for the stagnation point convective and radiative heat flux for objects with finite radius of curvature as a function of ρ_{air} and V. Convective heat flux correlations are given for a speed range of 3 to 17 km/s, whereas radiative heat flux correlation is only available for a speed range of 9.5 to 17 km/s. The correlations are only valid for densities between 1e-5 and 5e-3 kg/m^3 and radius of curvature between 0.2 and 10 m. Radiative heat transfer is assumed to be zero at speeds between 3 and 9.5 km/s and no heat transfer is included under speeds of 1.5 km/s.

At entry conditions other than the ones described above, we use the analytical and theoretical models for stagnation point convective and radiative heat flux. The convective heat flux is computed using the Fay-Riddell[21] relation given as:

$$\dot{Q}_C = 0.94\,(\rho_w \mu_w)^{0.1}\,(\rho_s \mu_s)^{0.4}\,(h_s - h_w)\sqrt{\left(\frac{du_e}{dx}\right)_s} \tag{10}$$

where $[\rho_w, \rho_s]$, $[\mu_w, \mu_s]$, and $[h_w, h_s]$ are density, viscosity, and enthalpy at the wall and stagnation point, respectively, and the last term is the velocity gradient at the stagnation point computed as:

$$\sqrt{\left(\frac{du_e}{dx}\right)_s} = \frac{1}{r_N}\sqrt{\frac{2\left(p_s - p_\infty\right)}{\rho_s}} \tag{11}$$

where (du_e/dx) is the velocity gradient, and p_s and p_∞ are stagnation point and free stream pressure, respectively.

The radiative heat flux is computed using the theoretical model given as:

$$\dot{Q}_R = \sigma k T_{shock}^4 \tag{12}$$

where σ is the emissivity, k is the Boltzmann constant, T_{shock} is the gas temperature just downstream of the shock. Because of the high temperature encountered during atmospheric entry, the value of emissivity if assumed to be always close to unity. The temperature just downstream of the shock or the shock layer temperature for radiative heat flux is computed by extrapolating the relation of Anderson[22] for chemically reacting gas in equilibrium to NEO re-entry velocities and assuming radiative equilibrium at approximately 25k Kelvin. Anderson's relation and the model used in the module are shown in Figure 4. In the atmospheric entry community, the heat flux distribution over

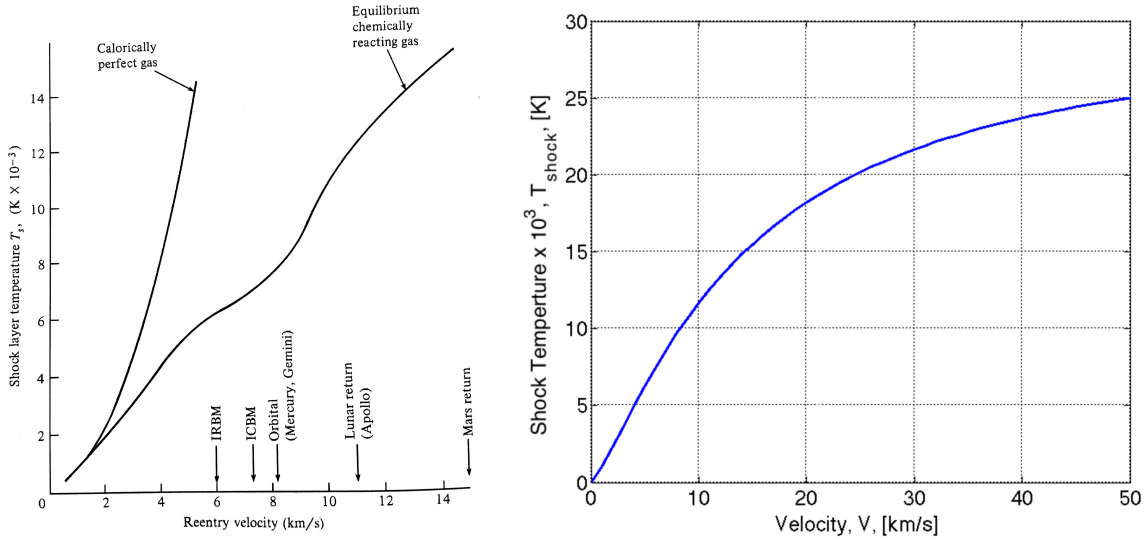

(a) (b)

Figure 4: (a) Shock layer temperature a chemically reacting gas in equilibrium as a function of velocity as given by Anderson [15], and (b) Anderson′s shock layer temperature extended to possible NEO re-entry velocities.

a spherical surface as a function the stagnation point heat flux is typically computed using one of the following two surface distributions:

$$Q(\theta) = Q_s(0.1 + 0.9cos\theta) \tag{13}$$

$$Q(\theta) = Q_s(0.7cos\theta) \tag{14}$$

The distributions in Eq.13 and Eq.14 result in a total effective heat transfer to the object of close to 25% and 17% of the stagnation heat flux, respectively. Under a conservative approach, the current work assumes the total effective heat transfer to be 10% of the stagnation point heat flux. A different values can easily be adopted depending on the requirements. The rate of ablation for the current work therefore becomes:

$$\dot{m} = -\frac{0.1(Q_R + Q_C)}{Q_{ab}} \tag{15}$$

Successive Fragmentation Model

A fragmentation event is modeled as a function of the stagnation pressure of the airflow free stream and the compressible strength of the asteroid material. A fragmentation occurs if the dynamic pressure exceeds the compressive strength of the material:[23]

$$\rho_{air} V^2 > \sigma_{com} \tag{16}$$

where σ_{com} is the compressive strength of the parent object. The compressive strength of the original parent object and the relative size of the fragmented pieces after each event are treated as uncertain parameters. Each fragmentation event is assumed to result into only two children, which allows significant simplification of the problem. The size of the smaller fragment after each fragmentation event is modeled with a uniform distribution in the size range of 0-50% of the parent. The number of successive fragmentation events are not limited but are based solely on the condition in Eq. 16 and the post-fragmentation structural strength of the pieces calculated using the model of Weibull[23] as follows:

$$\sigma_c = \sigma_p \left(\frac{m_p}{m_c} \right)^{\alpha} \tag{17}$$

where [σ_c,σ_p] and [m_c,m_p] are compressive strength and mass of the child and parent, respectively, and α is a scale factor. The scale factor, α, is another parameter considered uncertain.

Fragment Interaction and Lateral Velocity Model

Each successive fragmentation event is assumed to result in only 2 children with the small fragment given a small lateral velocity relative to the parent. The post fragmentation velocity of the second (larger) fragment is derived from conservation of momentum. The lateral velocity of separation is calculated based on the following relation of Passey and Melosh [12]:

$$V_T = \sqrt{C \frac{r_1}{r_2} \frac{\rho_{air}}{\rho_m}} V \tag{18}$$

where V_T is the final lateral velocity, C is a constant that Passey and Melosh[24] determined through examination of various terrestrial crater fields to lie between 0.03 and 2.5, r_1 is the size of the larger fragment, r_2 is the size of the smaller fragment, and m is the object material density. Laurence et al.,[17] performed an experimental and computational investigation into the unsteady separation behavior of two spherical objects under aerodynamics. Using experimental and computational analysis they derived the normalized separation velocity as a function of the ratio of the size of the fragments. Figure 4 shows the normalized separation velocity as a function of the fragment size ratio and Mach number. The data of Laurence et al.,[17] is extrapolated to Mach numbers typical of

small NEOs. We assume an asymptotic convergence to the solution for higher Mach (velocities) to Mach 25 values. The normalized separation velocity is used to compute the constant C using the following relationship:

$$C = V_T'^2 \frac{r_2}{r_1} \tag{19}$$

which is then used to compute the Lateral velocity as per the model of Passey and Melosh.[24] It should be noted that the lateral velocity depends on the relative orientation of the two fragments at separation. However, since the orientation is not known apriori, the proposed probabilistic analysis is assumed to mitigate that uncertainty.

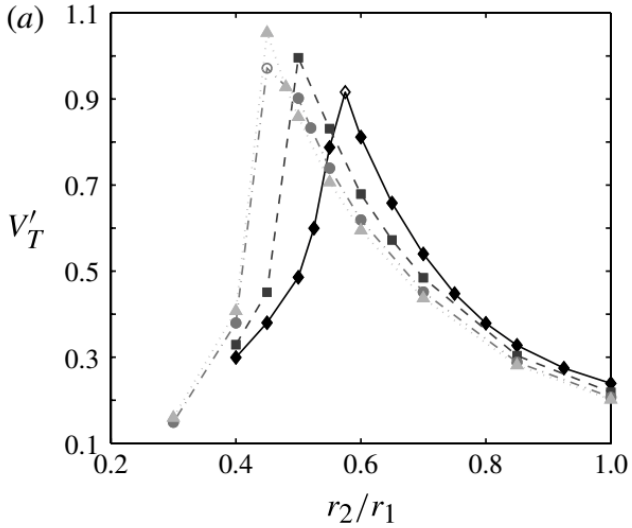

Figure 5: Normalized separation velocity as a function of fragment size ratio. diamond, M = 4; square, M = 6; circle, M = 10; triangle, M = 25.[17]

HDMR based uncertainty quantification approach

The most general way to perform uncertainty propagation (UP), as well as global sensitivity analysis, is to use the Monte-Carlo (MC) approach, which basically follows three main steps: 1) sample the input random variable(s) from their known or assumed (joint) Probability Density Function (PDF), 2) compute deterministic output for each sampled input value(s), and 3) determine the statistical characteristics of the output distribution (e.g. mean, variance, skewness). The MC method has the property that it converges to the exact stochastic solution when the number of samples $n \to \infty$. In practice the value of n can be a finite number, but to have a highly converged process it should be very high, causing excessive computational costs (even for modern computers).

A way to reduce the computational time of the UP process could be to build a less expensive surrogate of the model and then use it to propagate the uncertainty. Among the surrogate based approaches, there are the Stochastic Collocation (SC) method, the Polynomial Chaos (PC),[25] and the Kriging surrogate model.[26] These methods are non-intrusive by nature, because they consider the model as a black box and try to approximate the implemented function. One of the major issues of the surrogate based approaches is the so called Curse of Dimensionality (CoD),[27] which limits

their use to problems with low dimensionality. The cut-High Dimensional Model Representation (cut-HDMR)[28] was developed to decouple the interaction effects of chemical systems.

In this work a new method for UP is used and compared to the results given by MC. The used approach decomposes the stochastic space into sub-domains, which are then interpolated separately by a selected interpolation technique. Each interpolating model is built accordingly to the outcomes of a new derivation of the cut-HDMR. The contribution of each independent sub-domain to the final response is evaluated, and only important sub-domains are sampled and interpolated, causing a dramatic reduction of the necessary number of samples for high dimensional spaces.

The HDMR based approach[12] proposed for this study is based on the cut-High Dimensional Model Representation (cut-HDMR) decomposition, and it allows a direct cheap reconstruction of the quantity of interest and analyses similar to an ANOVA (Analysis Of Variance) decomposition [23]. Basically, the function response, $f(x)$, is decomposed in a sum of contributions given by each stochastic variable and each one of their interactions through the model, considered as increments with the respect the nominal response, f_c:

$$f(x) = f_c + \sum_{i=1}^{n} dF_i + \sum_{1 \leq i < j \leq n} dF_{ij} + ... + dF_{1,2,...,n} \tag{20}$$

where n is the number of variables.

A surrogate model representation can be independently generated for each element of the sum (called Increment Functions) and only for the non-zero elements, thus greatly reducing the complexity of sampling and building the model. Moreover, the contribution of each term of the sum to the global response can be quantified independently so that higher order interactions with low or zero contribution can be neglected already by analyzing the lower order terms. More detailed info can be found in the above mentioned article.[12]

Use of the HDMR approach for atmospheric entry uncertainty quantification

As briefly mentioned in the introduction, the HDMR approach is used here to learn the dynamics and evolution of the entering objects through the atmosphere. Given a general enough set of initial conditions, in terms of states and object properties, such as strength, density and heat of ablation, the learning technique is able to learn, and then generalise, the state of the object at a major event, through a supervised leaning approach. That is, given the state and properties at time $t_0 = 0$ as $S_0 = [h_0, v_0, \gamma_0, \chi_0, \phi_0, \lambda_0, m_0]$, and $P_0 = [\sigma_{com,0}, \rho_{m,0}, Q_{ab,0}]$, where h is altitude, v is velocity, γ is flight path angle, χ is direction angle, ϕ is latitude, λ is longitude, m is mass, σ_{com} is compressive strength of the material, ρ_m is the material density, and Q_{ab} is the heat of ablation; the learning technique is able to learn the change in state, $\Delta S = [\Delta h, \Delta v, \Delta\gamma, \Delta\chi, \Delta\phi, \Delta\lambda, \Delta m]$, up to the first major event. This approximated model can then be used to predict the final state of the object as $S_f = [h_f = h_0 + \Delta h, v_f = v_0 + \Delta v, \gamma_f = \gamma_0 + \Delta\gamma, \chi_f = \chi_0 + \Delta\chi, \phi_f = \phi_0 + \Delta\phi, \lambda_f = \lambda_0 + \Delta\lambda, m_f = m_0 + \Delta m]$. Once the final state is approximated, the check on h_f, v_f, and m_f, can tell which major event occurs:

- if condition (16) holds, and $h_f > 0$ and $m_f > 0$, then the event is *fragmentation*;
- else if $h_f \approx 0$, then the event is *ground impact*;
- else if $m_f \approx 0$, then the event is *evaporation*.

For this preliminary work, the HDMR approach has been used to learn the dynamics and evolution of the enetring objects for the range of initial states and properties described in Table 1

S_0/P_0	**Lower bound**	**Upper Bound**
$h_0[km]$	1	120
$v_0[m/s]$	10	$7e4$
$\gamma_0[deg]$	-80	-10
$m_0[kg]$	$1e4$	$1e8$
$\sigma_{com,0}[Pa]$	$1e6$	$1e8$
$Q_{ab,0}[J/kg]$	$1e6$	$1e7$
$\rho_{m,0}[kg/m^3]$	$3e3$	$4e3$

Table 1: Range of initial states and properties for the HDMR based learning approach

For this preliminary work, initial values of flight direction angle, latitude and longitude are kept constant for the learning phase. More specifically, $\chi_0 = 90[deg]$, $\phi_0 = 0$, $\lambda_0 = 0$.

RESULTS

The approach described in the previous section has been applied to an example of entry case, and compared to the propagation of objects and fragments via numerical integration of the dynamical set of equations in terms of both accuracy and computational cost. The uncertainties considered on the initial state at $120km$ altitude for the study case are summarized in Table 2.

Stochastic variable	Lower bound	Upper Bound
$v_{0,120}[m/s]$	$17e3$	$19e3$
$\gamma_{0,120}[deg]$	-45	-35
$m_0[kg]$	$9e6$	$11e6$
$\sigma_{com,0,120}[Pa]$	$9e6$	$11e6$
$Q_{ab,0,120}[J/kg]$	$1e6$	$3e6$
$\rho_{m,0,120}[kg/m^3]$	$3e3$	$4e3$

Table 2: Bounds of uniform PDFs considered for the test case

From the PDFs in Table 2, 100 samples have been extracted and the uncertainty analysis both with standard propagation (i.e., the integration of the dynamical equations 1-6) and the HDMR based propagation have been carried out. The results are analyzed and compared by means of Figures 6-10, reporting on the left the statistical results (pdf) obtained via standard integration of the dynamical equations, and on the right the same results obtained via HDMR based approach.

The HDMR approach, instructed over a very broad range of input parameters, over-predicts both Δh and (especially) Δv, resulting into a smaller number of fragmentation events, occurring at lower

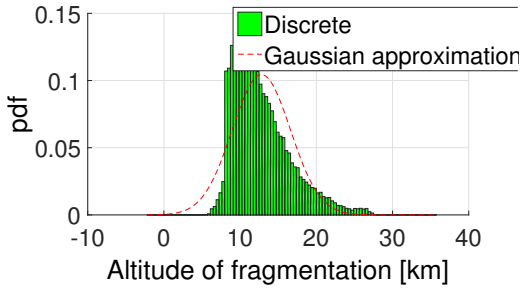

(a) Standard integration of the dynamical equations

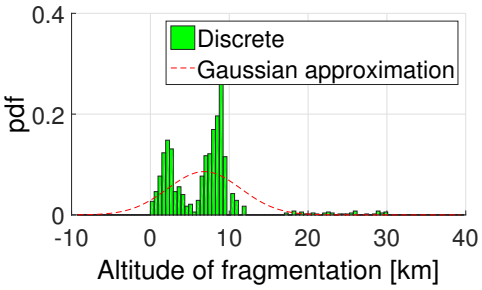

(b) HDMR based approach

Figure 6: Altitude of fragmentation events as predicted via standard integration of the dynamical equations and via HDMR based approach

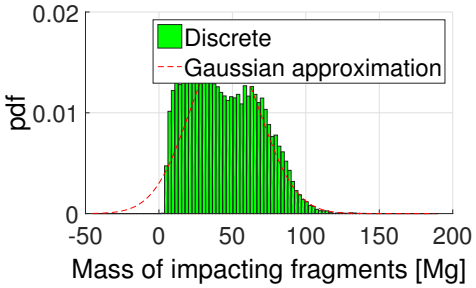

(a) Standard integration of the dynamical equations

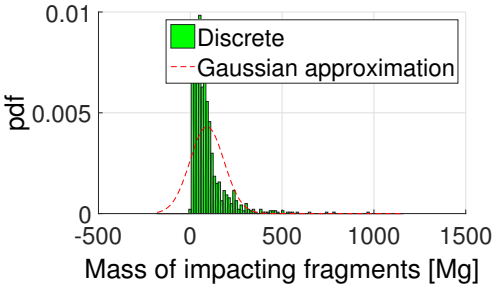

(b) HDMR based approach

Figure 7: Mass of impacting fragments as predicted via standard integration of the dynamical equations and via HDMR based approach

altitudes (Fig. 6). For this reason, fragments with higher mass impact the ground (Fig. 7) at a lower distance from the entry point (Fig. 8) and with less lateral spreadiness (Fig. 9).

Since the underestimation of the final velocity (at impact) compensates the overestimation of the mass of the impacting objects, the distribution of the kinetic energy of the impacting fragments obtained by the HDMR approach (Fig. 10b) is comparable with the one obtained via standard integration (Fig. 10a).

When the accuracy of the approximation is enhanced, the results obtained by the HDMR based approach tend to the ones obtained by the standard propagation. This can be seen in Tables 3 and 4, where the statistical characteristics of the relevant distributions are compared in the cases: a) standard propagation (STD-P), b) first set of HDMR based propagation (HDMR-1), c) HDMR based propagation with improved accuracy on the approximation of the variation of the velocity per leg (HDMR-2).

With the only improvement of the approximation in terms of variation of velocity for each leg, Δv, the statistical performance of the HDMR based propagation tend to those obtained via standard propagation, with a much closer matching in terms of mass of the impacting fragments, as can be seen also in Figure 11. Due to the broad range of input variables, the precise approximation of both Δh and Δv has been proved to be quite difficult, and the current efforts are devoted to the development of a partitioning strategy, to apply the HDMR learning approach to multiple, but

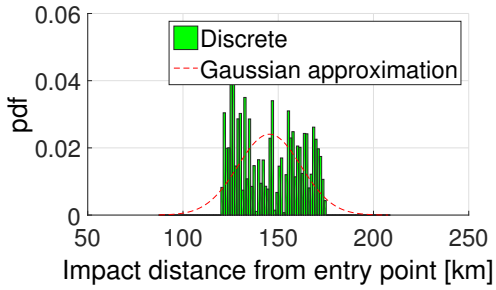

(a) Standard integration of the dynamical equations

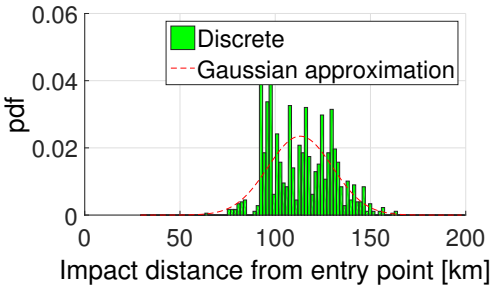

(b) HDMR based approach

Figure 8: Longitudinal position of impacting fragments with respect to the projection of the atmospheric entry point as predicted via standard integration of the dynamical equations and via HDMR based approach

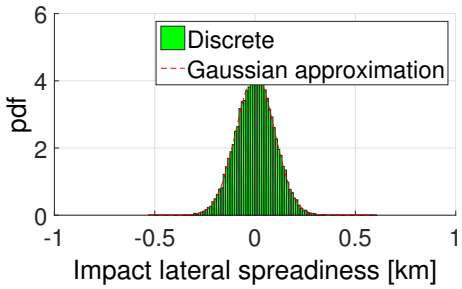

(a) Standard integration of the dynamical equations

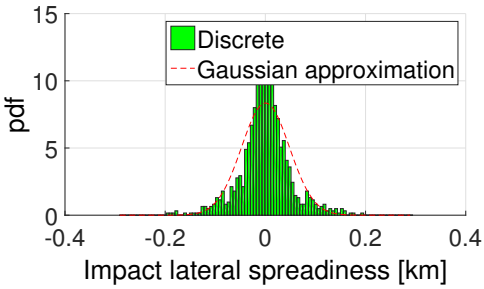

(b) HDMR based approach

Figure 9: Lateral position of impacting fragments with respect to the projection of the atmospheric entry point as predicted via standard integration of the dynamical equations and via HDMR based approach

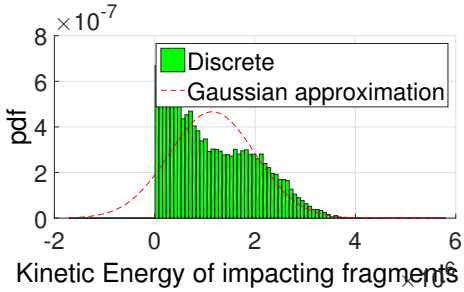

(a) Standard integration of the dynamical equations

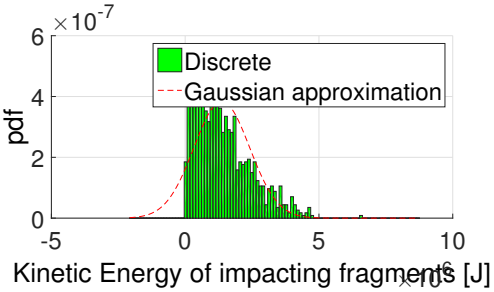

(b) HDMR based approach

Figure 10: Kinetic energy of impacting fragments as predicted via standard integration of the dynamical equations and via HDMR based approach

	STD-P	HDMR-1	HDMR-2
Mass of impacting fragments [Mg]	44.784	90.903	33.204
Impact: distance from entry point [km]	145.37	113.12	115.13
Impact: lateral spreadiness [km]	0.0010194	0.00022265	0.0033976
Altitude of fragmentation [km]	12.785	6.8299	7.7902

Table 3: Mean values of the relevant distributions compared in the cases: a) standard propagation (STD-P), b) first set of HDMR based propagation (HDMR-1), c) HDMR based propagation with improved accuracy on the approximation of the variation of the velocity per leg (HDMR-2)

	STD-P	HDMR-1	HDMR-2
Mass of impacting fragments [Mg]	24.342	92.684	21.956
Impact: distance from entry point [km]	16.58	16.996	11.253
Impact: lateral spreadiness [km]	0.095519	0.047816	0.075885
Altitude of fragmentation [km]	3.8195	4.6429	3.4126

Table 4: Standard deviation values of the relevant distributions compared in the cases: a) standard propagation (STD-P), b) first set of HDMR based propagation (HDMR-1), c) HDMR based propagation with improved accuracy on the approximation of the variation of the velocity per leg (HDMR-2)

smaller domains, while still containing the overall computational costs to less than 10% of the cost of the analysis based on standard propagation.

Note, that due to the range of the input states and properties used, the standard integration is still adopted when altitude, velocity and mass become too small, or when the strength of the fragments becomes too high (see Eq. 16).

CONCLUSION

An approximation technique, able to handle high dimensional models, has been applied to the uncertainty bases simulation of entering objects experiencing both ablation and fragmentation, with the aim to considerably reduce the computational time usually requested by this kind of simulation. A HDMR based approach is used to learn the dynamics and evolution of the entering objects through the atmosphere, i.e., learn, and then generalise, the state of the entering objects at a major event, thus avoiding the use of standard numerical propagation.

Preliminary results show that the proposed approach has the potential to significantly reduce the computational costs related this kind of simulation based analyses, but the implementation of the method should be improved to increase the accuracy of the approximation of the probability density function for the relevant events, such as ground impact and fragmentation.

Current efforts are made in this direction, and the next step will be the development of a learning strategy based on the partition of the input domain into smaller and more manageable ones.

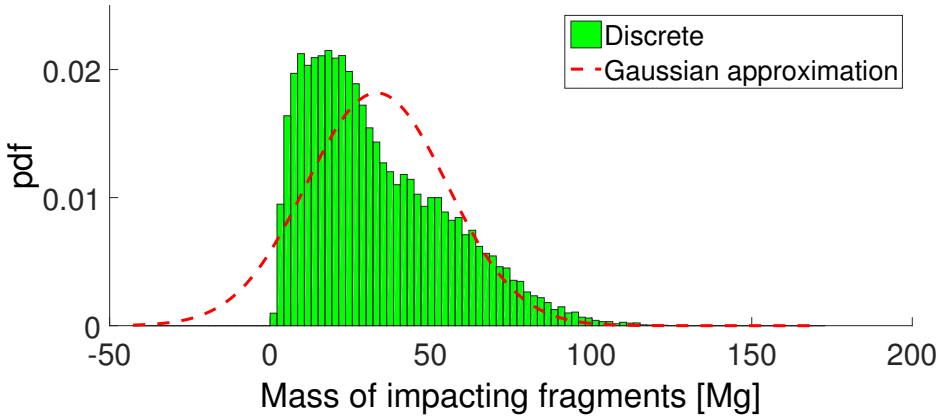

Figure 11: Mass of impacting fragments as predicted via HDMR based approach with improved accuracy on the approximation of the variation of the velocity during each leg (HDMR-2).

ACKNOWLEDGMENT

Funding for Piyush Mehta is provided by the European Commission through the Marie Curie Initial Training Network (ITN) STARDUST under grant number 317185. Partial support for Martin Kubicek is provided by 'OPTIMAD Engineering Srl'.

REFERENCES

[1] O. P. Popova, P. Jenniskens, V. Emel'yaneko, and e. al., "Chelyabinsk Air- burst, Damage Assessment, Meteorite Recovery, and Characterization," *Science*, Vol. 342, No. 6162, 2013, pp. 1069–1073.

[2] Q. Schiermeier, "Risk of massive asteroid strike underestimated," Nature News, Nature Publishing Group, November 2013.

[3] W. Cooke, "Orbit of the Russian Meteor," NASA blogs, February 2013.

[4] T. Malik, "Russian Meteor Blast Bigger Than Thought," NASA says, Huffington Post, February 2013.

[5] T. J. Takata and J. D. O'Keefe, "Impact of Comet Shoemaker-Levy 9 on Jupiter," *Geophysical Research Letters*, Vol. 21, 1994, pp. 1087–1090.

[6] M. B. Boslough, D. A. Crawford, A. C. Robinson, and T. G. Trucano, "Mass and penetration depth of Shoemaker-Levy 9 fragments from time-resolved photometry," *Geophysical Research Letters*, Vol. 21, 1994, pp. 1555–1558.

[7] M. M. M. Low and K. J. Zahnle, "Explosion of comet Shoemaker- Levy 9 on entry into the Jovian atmosphere," *Astronomical Journal*, Vol. 21, 1994, pp. L33–L36.

[8] I. V. Nemtchinov, N. A. Artem'eva, I. B. Kosarev, and V. V. S. e. al., "Luminosity of the bolides created by SL-9 comet fragments in the Jovian atmosphere," *International Journal of Impact Engineering*, Vol. 20, 1997, pp. 591–599.

[9] D. G. Korycansky, K. J. Zahnle, and M. M. M. Law, "High-resolution calculations of asteroid impacts into the Venusian atmosphere," *Icarus*, Vol. 146, 2000, pp. 387–403.

[10] V. V. Shuvalov and N. A. Artemieva, "Numerical modeling of Tunguska-like impacts," *Planetary and Space Science*, Vol. 50, 2002, pp. 181–192.

[11] P. M. Mehta, E. Minisci, and M. Vasile, "Break-up Modeling and Trajectory Simulation under Uncertainty for Asteroids," *4th IAA Planetary Defense Conference*, Frascati, Roma, April 2015.

[12] M. Kubicek, E. Minisci, and M. Cisternino, "High dimensional sensitivity analysis using surrogate modeling and High Dimensional Model Representation," *International Journal for Uncertainty Quantification*, Vol. 5, No. 5, 2015, pp. 393–414.

[13] P. M. Mehta, M. Kubicek, E. Minisci, and M. Vasile, "Debris Re-entry Modeling using High Dimensional Derivative Based Uncertainty Quantification," *AAS/AIAA Astrodynamics Specialist Conference*, Vail, Colorado, USA, August 2015.

[14] A. M. Brandis and C. O. Johnston, "Characterization of Stagnation-Point Heat Flux for Earth Entry," *45th AIAA Plasmadynamics and Lasers Conference, AIAA Aviation*, Atlanta, Georgia, USA, June 2014.

[15] V. A. Bronshten, *Physics of Meteoric Phenomena*. Izdatel'stvo Nauka translated by D. Reidel Publishing Co., 1983.

[16] V. I. Tsvetkov and A. Y. Skripnik, "Atmospheric fragmentation of meteorites according to the strength theory," *Sol. Syst. Res.*, Vol. 25, 1991, pp. 273–279.

[17] S. J. Laurence, N. J. Parziale, and R. Deiterding, "Dynamical separation of spherical bodies in supersonic flow," *J. Fluid Mech.*, Vol. 713, 2012, pp. 159–182.

[18] I. Newton, *Principia*. University of California Press: Translated by Mote, 1946.

[19] P. M. Mehta, E. Minisci, M. Vasile, *et al.*, "Sensitivity Analysis towards Probabilistic Re-Entry Modeling of Spacecraft and Space Debris," *Proceeding of the AIAA Modeling and Simulation Technologies Conference*, Dallas, TX, June 2015. AIAA 2015-3098.

[20] "U.S. Standard Atmosphere, 1976," Tech. Rep. NOAA-S/T 76-1562, National Oceanic and Atmospheric Administration, Washington, DC: U.S. Government Printing Office, 1976.

[21] J. A. Fay and F. R. Riddell, "Theory of Stagnation Point Heat Transfer in Dissociated Air," *Journal of the Aeronautical Sciences*, Vol. 25, No. 2, 1958, pp. 73–85.

[22] J. D. Anderson. American Institute of Aeronautics and Astronautics, editor = D. Reidel Publishing Co., title = Hypersonic and High Temperature Gas Dynamics, year = 1989,.

[23] W. Weibull, "A statistical distribution function of wide applicability," *Journal of Applied Mechanics*, Vol. 10, 1951, pp. 140–147.

[24] Q. R. Passey and H. J. Melosh, "Effects of atmospheric breakup on crater field formation," *Icarus*, Vol. 42, No. 2, pp. 211–233.

[25] M. Eldred and J. Burkardt, "Comparison of nonintrusive polynomial chaos and stochastic collocation methods for uncertainty quantification," *47th AIAA Aerospace Sciences Meeting including The New Horizons Forum and Aerospace Exposition*, Orlando,Florida, January 2009.

[26] K. T. Fang, R. Li, and A. Sudjianto, *Design and Modeling for Computer Experiments*. Chapman and Hall/CRC press, 2006.

[27] R. E. Bellman, *Adaptive Control Processes: A Guided Tour*. Princeton University Press, 1961.

[28] J. A. Shorter, P. C. Ip, and H. Rabitz, "An efficient chemical kinetics solver using high dimensional model representation," *J. Phys. Chem.*, Vol. 103, 1999, pp. 7192–7198.